Journal of Molecular Liquids, Volume 316, October 2020, Article number 113863
DOI: 10.1016/j.molliq.2020.113863

High CO_2 Absorption in New Amine Based-Transition-Temperature Mixtures (Deep Eutectic Analogues) and Reporting Thermal Stability, Viscosity And Surface Tension: Response Surface Methodology (RSM)

Hosein Ghaedi [a], Ming Zhao [a,*], Peter T. Clough [b], Edward J. Anthony [c], Paul S. Fennell [d]

[a] School of Environment, Tsinghua University, Beijing 100084, China

[b] Energy and Power Theme, Cranfield University, Cranfield, Bedfordshire MK43 0AL, UK

[c] Department of Chemical Engineering, Imperial College London, South Kensington, London, SW7 2AZ, UK

[*] Corresponding author. Email: ming.zhao@tsinghua.edu.cn; Tel/Fax: +861062784701.

Abstract

To study CO_2 capture potential, *n*-methyl diethanolamine (MDEA) was used to prepare three types of transition-temperature mixtures (TTMs) by mixing methyltriphenylphosphonium bromide (MTPPB) as a hydrogen bond acceptor (HBA) and MDEA as a hydrogen bond donor (HBD) in molar ratios of 1:7, 1:10 and 1:16 HBA to HBD. Fourier transform infrared spectroscopy (FT-IR) results showed that TTMs have almost similar spectra to their HBD (MDEA) with different levels of transmittance and exhibit similar behavior. From the experimental results, it was found that the thermal stability, viscosity and surface tension of TTMs decreased as the concentration of MDEA in the mixture increased. According to response surface methodology (RSM) models and analysis of variance (ANOVA), temperature and molar ratio had a great effect on the viscosity and surface tension of TTMs. The final part of this research was the measurement of CO_2 solubility in TTMs at 303.15 K at pressure up to 1.35 MPa. It was found that CO_2 solubility in TTMs was enhanced as the MDEA quantity increased in the mixture up to 1:10 mole ratio. However, by increasing MDEA concentration to 16:1 mole ratio, there was a decreasing trend in the CO_2 solubility data. Also, all TTMs, particularly TTM containing 10:1 mole MDEA (MTPPB-MDEA 1:10) exhibited an equilibrium loading capacity approaching 1 mole CO_2 per mole solvent at high pressure, revealing

Published by Elsevier. This is the Author Accepted Manuscript issued with: Creative Commons Attribution Non-Commercial No Derivatives License (CC:BY:NC:ND 4.0).
The final published version (version of record) is available online at DOI:10.1016/j.molliq.2020.113863. Please refer to any applicable publisher terms of use.

their high potential for CO_2 capture. A comparison showed that the CO_2 solubility in the studied solvents was higher than that of existing deep eutectic solvents (DESs) and other TTMs as well as several ionic liquids (ILs) to date. To the best of our knowledge, this is the first study to report the CO_2 solubility in phosphonium-base TTMs containing MDEA.

Keywords: Transition-temperature mixtures; Fourier transform infrared spectroscopy; Thermogravimetric analysis; viscosity; surface tension; CO_2 solubility.

▪ INTRODUCTION

CO_2 is the main greenhouse gas (GHG), which is released through human activities, for example, burning fossil fuels and deforestation, as well as natural sources (i.e. volcanic eruptions). According to Mauna Loa Observatory data, the emissions of CO_2 have dramatically increased over the last 50 years and atmospheric concentration reached values around 409.02 ppm in October 2019.[1] The high CO_2 concentration is leading to dramatic changes in global temperature and climate change. It is projected that if CO_2 emissions are not reduced quickly, the global surface temperature might rise 2-5 °C by the end of this century.[2] Therefore, the influence of the steadily growing CO_2 concentration released to the atmosphere has received increasing scientific attention. Carbon capture and storage (CCS) technology offers viable solutions to tackle problems related to emissions of GHGs.[3,4] The first step in the CCS chain is the capture of CO_2. There are several strategies to reduce CO_2 emissions: post-combustion, pre-combustion, oxy-fuel combustion, and electrochemical separation. Post-combustion capture can be regarded as the most straightforward technology among these available technologies.[5] In this case, chemical absorption using amine-based solvents is the most suitable technology for reduction of CO_2 emissions in industrial processes such us fossil fuels power plants, cement production, and iron and steel manufacturing.[6-9] Amine-based chemical absorption technology was developed to remove CO_2 about 70 years ago.[10] There are, however, several inherent drawbacks related to using amine solvents which limit the use of amine-based technology, especially, the large energy requirements for solvent regeneration, formation of corrosive

byproducts, solvent losses and solvent degradation products,[11-19] and these inherent drawbacks limit the use of amine-based technology. Therefore, the design of alternative solvents for CO_2 removal is of high importance and researchers are trying to synthesize and explore new efficient solvents as alternatives to traditional CO_2 absorbents.

Among the many possibilities, ionic liquids (ILs), deep eutectic solvents (DESs) and transition-temperature mixtures (TTMs) have been considered and attracted wide attention as potential solvents for CO_2 capture. ILs have been proposed for many applications especially CO_2 capture due to many unique characteristics; however, they suffer several disadvantages which have limited their use in large-scale industrial applications including potential toxicity, the creation of large amounts of waste, availability and cost issues, purification and complex reaction steps, poor biodegradability, high viscosity, and low CO_2 loading capacity.[20-23]

DESs and TTMs have emerged as possible alternatives to both conventional solvents and ILs. In 2003, Abbott *et al.* explored DESs by a combination of a range of quaternary ammonium salts and urea.[24] TTMs combining different natural carboxylic acids, amino acids, choline chloride, and other environmentally benign starting constituents were introduced by Francisco *et al.* in 2012.[25] They have several solvent properties similar to ILs and some potential advantages over ILs, including low cost, easy preparation routes, good renewability, and low toxicity. The main differences between these solvents and ILs are: (1) DESs and TTMs can be prepared from non-ionic species in some cases; and (2) DESs and TTMs comprise both ionic and neutral species while ILs are entirely made of ions.[26]

Both DESs and TTMs are composed of two or more components, namely hydrogen bond acceptors (HBAs) and hydrogen bond donors (HBDs) which can associate with each other through the hydrogen bonding interactions. The difference between these solvents is that TTMs show only a glass transition-temperature while DESs display not only glass transition temperature but also a freezing point in differential scanning calorimetry (DSC) curves.[22,27,28] Because of the tunable

composition of TTMs, it is possible to control their physicochemical properties and phase behavior. Moreover, most TTMs have other advantages including a wide liquid range, low volatility, non-flammability, biocompatibility, biodegradability and above all, easy preparation without further purification.[27-29] TTMs have been used in different areas, for example, as the entrainers for extractive distillation,[30] and simulation of ethanol-water systems separation,[31] the antioxidant phenolics extraction from industrial cereal solid wastes,[32] metal extraction,[33] polyphenols extraction from *Moringa oleifera* leaves,[34] and from olive leaves,[35] biomass delignification,[36,37] lignin modification,[38] the electrodeposition of zinc,[39] and CO_2 capture.[22,40]

In order to establish the possible use of TTMs in chemical engineering and industrial processes, it is necessary to know and collect their thermo-physical properties. To date, the thermo-physical characterization of TTMs is inadequate and there exist minimal data on these properties, particularly viscosity, surface tension, and thermal stability data; therefore, there is a need to collect thermo-physical data for TTMs. On the other hand, CO_2 solubility in DESs and TTMs is not very good. To overcome this limitation, synthesizing solvents with better CO_2 absorption performance is also required. Since TTMs have tunable properties, it is possible to prepare new solvents using different amines as HBDs to improve CO_2 absorption. Alkanolamines, for instance, monoethanolamine (MEA), diethanolamine (DEA), *n*-methyldiethanolamine (MDEA), and 2-amino-2-methyl-1-propanol (AMP) are widely used in industries as sweetening agents. To investigate the possibility of improving CO_2 solubility in TTMs, therefore, MDEA (a tertiary alkanolamine) was used. MDEA has several advantages such as a high CO_2 loading capacity (1 mole CO_2 per mole of MDEA), low energy requirement for regeneration, lower vapor pressure and corrosiveness, better thermal and chemical stability.[41,42] Therefore, in this study, TTMs were prepared by mixing methyltriphenylphosphonium bromide (MTPPB) as HBA and MDEA as HBD in three molar ratios of 1:7, 1:10 and 1:16 HBA/ HBD. The main objectives of this study are: (1) analysis of the functional groups and hydrogen bonding; (2) investigation of fundamental thermo-physical properties of

solvents namely viscosity, surface tension, and thermal stability; and (3) measurement of CO_2 solubility.

▪ EXPERIMENTAL SECTION

Chemicals and Gases

MDEA was purchased from Merck Sdn Bhd. MTPPB was supplied by Angene International Limited. CO_2 and N_2 as the purified gases were used in this research work. CO_2 and N_2 were purchased from Malaysian Oxygen Berhad and Malaysian Weld Gas Enterprise, respectively. Table S1 provides the details of pure chemicals and gases utilized in this research work. Table 1 presents the abbreviation of TTMs and their individual components together with the symbol, molecular weight, molar ratio, and glass transition temperature. The chemical structures of MTPPB and MDEA are shown in Fig. S1.

Table 1 . The Composition and T_g of TTMs

Solvent		HBA		HBD		Molar ratio		Glass transition (T_g / °C) [d]
Symbol	M_{TTM} [a]	Abbreviation	M_{HBA} [b]	Abbreviation	M_{HBD} [c]	HBA	HBD	
TTM_1	148.920	MTPPB	357.22	MDEA	119.163	1	07	-100.33
TTM_2	140.805	MTPPB	357.22	MDEA	119.163	1	10	-100.54
TTM_3	133.166	MTPPB	357.22	MDEA	119.163	1	16	-101.39

[a] Molecular mass of TTM in $g.mol^{-1}$ (formula is available in the previous work).[43] [b] Molecular mass of HBA in $g.mol^{-1}$. [c] Molecular mass of HBD in $g.mol^{-1}$. [d] Glass transition temperatures of TTMs were taken from previous work.[28]

DES Preparation

TTMs were synthesized easily according to the preparation process reported in the previous works.[27,28] In brief, MTPPB (solid) as HBA was mixed with MDEA as HBD in three molar ratios

of 1:7, 1:10, and 1:16 HBA/HBD using a hot plate magnetic stirrer in sealed bottles and stirred at 400 rpm and heated up to 373 K. After around 1 h, the solvents became homogeneous, uniform and stable with no precipitation. All solvents were kept in tightly-sealed bottles and a humidity-controlled environment to prevent moisture and any contamination from the outside atmosphere. The TTMs were used without any further purification.

Characterization

In order to identify the transformations resulting from the formation of TTMs and analyze functional groups of TTMs, MTPPB, and MDEA, a Thermo Scientific™ Nicolet™ iS 10 FT-IR spectrometer (KBr disc, resolution 4 and apodization function of Norton-Beer) was employed at ambient temperature. The FT-IR spectra of samples were recorded at the wavenumbers from 4000 cm^{-1} to 600 cm^{-1}.

For thermogravimetric analysis (TGA), a Perkin-Elmer (STA 6000) instrument was used to measure the thermal decomposition temperatures (T_{dcp}) of all samples with an accuracy of temperature control better than ±0.5 K. The samples were placed in a small pan under N_2 atmosphere with a flow rate of 20 $mL.min^{-1}$ and heated at a rate of 10 $K.min^{-1}$ in a temperature range from 298 K to 1100 K.

A rotational automated viscometer Anton Paar Stabinger SVM3000 with cylindrical geometry was used for measurement of viscosity of TTMs and MDEA at atmospheric pressure. Further details on the instrument and measurement procedure are found in the literature.[44,45] According to the manufacturer, it allows viscosity measurements over the temperature range from 243.15 to 378.15 K, and in the viscosity range of 0.2 to 20 Pa.s. The viscosity meter was calibrated by the manufacturer, using several density and viscosity standard reference fluids. The uncertainty of temperature for the viscosity meter is ±0.02. The viscosities of HBD and TTMs were measured three times at atmospheric pressure and at temperatures ranging from 293.15 K to 353.15 K with an interval of 10 K. The final viscosity data are the average values of three measurements.

A video-camera based optical contact angle tensiometer (OCA 15 EC) was employed to determine the surface tension of TTMs and MDEA through a pendant drop method. The machine has a measuring accuracy of ±0.03 $mN.m^{-1}$. Additional details about the instrument and measurement procedure are available elsewhere.[46] The surface tensions of MDEA and TTMs were measured three times at atmospheric pressure and at temperatures ranging from 298.15 to 353.15 K. The final surface tension data are the average values of three measurements.

CO_2 Solubility Measurement

Pressure drop is an isochoric method commonly used for CO_2 solubility measurement in the solvents.[47,48] In this method, the solvent volume is maintained constant while the pressure in the equilibrium cell is monitored during CO_2 absorption by the solvent. A high-pressure solubility cell (SOLTEQ BP-22) was employed to measure CO_2 solubility in TTMs, as shown in Fig. S2. Details of this apparatus have been explained elsewhere.[49-52] A set of equations (Eqs. (S1)-(S7)) was used to calculate the CO_2 solubility,[49,50,53,54] as presented in the Supplementary Material.

Design of experiment (DOE)

Design of experiment (DOE) is an effective method to manipulate a process as opposed to observing a process.[55,56] Studying the influence of input factor(s) on the response(s) is highly important in a process. To do so, therefore, DOE was applied by selecting the user-defined option of response surface methodology (RSM). This efficient method of DOE can be also used for modeling and optimizing processes.[15,16,28,49,57-59] This method was applied to study the effect of temperature (T/K) and HBA mass fraction (w_{HBA}) as two important factors on the responses such as viscosity and surface tension of TTMs. Table S2 lists these input factors along with their respective levels. Tables S3 and S4 present the user-defined matrix for viscosity and surface tension, respectively. Three-dimensional (3-D) surface plots are created based on the developed regression models to study the effect of aforementioned factors on the responses. In this work,

Design Expert 10.0.4.0 was used to design the experiments and analyze the results. More detail on DOE is available in Supplementary Material (see Appendix A, section 2).

▪ RESULTS

FT-IR Analysis

The FT-IR spectra of the individual constituents (MTPPB and MDEA) and prepared solvents TTM_1, TTM_2 and TTM_3 are shown in Fig. S3 and Fig. 1, respectively. The hydrogen bonding interactions appear at the wavenumbers between 3800 cm^{-1} to 3100 cm^{-1}. The hydroxyl group of HBDs favors the hydrogen bonding between the anion of HBA and HBD. As evident in Fig. S3, the peak at the wavenumber of 3312.30 cm^{-1} is associated with hydrogen bonding interactions in pure MDEA. After the formation of TTMs, this absorption band shifted to a weaker band. From Fig. 1, OH stretching bands occurred at the wavenumbers of 3325.42 cm^{-1}, 3330.13 cm^{-1}, and 3345.22 cm^{-1} in TTM_1, TTM_2, and TTM_3, respectively. Indeed, a blue shift of OH stretching bands was observed. This indicates that adding MTPPB to MDEA decreased the strength of hydrogen bonds in new TTMs compared with pure MDEA.

On the other hands, the strength of hydrogen bonding between HBA and HBD increases by the fractional decrease in the OH covalent bonds wavenumbers. The wavenumbers of OH stretching vibrations in TTM_1, TTM_2, and TTM_3 are 3325.42 cm^{-1}, 3330.13 cm^{-1}, and 3345.22 cm^{-1}, respectively. Therefore, the lower OH stretching frequency in TTM_1 indicates that the hydrogen bonds inside TTM_1 are relatively stronger than those of TTM_2 and TTM_3.

Since MDEA is a tertiary amine, there are no N-H stretching bands in the spectrum of MDEA as well as in the spectra of the TTMs.

Normally, the bands at the wavenumbers of 2940-2915 cm^{-1} and 2870-2840 cm^{-1} are assigned to CH_2 stretching bands, while the CH_3 stretching bands appear in the vicinity of 2950-2975 cm^{-1} and 2885-2865 cm^{-1}. Since these bands are weak, they may not be distinguished in the spectrum.[60-64] In

pure MDEA, theses aliphatic stretching bands occurred in the region from 2945.32 cm^{-1} to 2841.04 cm^{-1}, as depicted in Fig. S3. From Fig. 1, these vibrations can be observed at almost the same region from 2946 cm^{-1} to 2840 in the case of all TTMs.

In tertiary amines, methyl and methylene groups next to the nitrogen atom result in bands at 2800 cm^{-1}.[60] From Fig. S3, this C-N stretching band appeared at the wavenumber of 2798.31 cm^{-1} in the spectra of MDEA. The peaks at the wavenumbers of 2797.31 cm^{-1} for TTM_1, 2795.95 cm^{-1} for TTM_2, and 2795.53 cm^{-1} for TTM_3 are ascribed to the C-N stretching band.

The wavenumbers between 1100 cm^{-1} and 1030 cm^{-1} are associated with C-O stretching.[65] For pure MDEA, the C-O stretching band occurred in two wavenumbers, 1031.89 cm^{-1} and 1078.46 cm^{-1}, as depicted in Fig. S3. According to Fig. 1, it is obvious that these vibrations occurred in two vicinities for all TTMs; 1031.37 cm^{-1} and 1077.86 cm^{-1} for TTM_1, 1031.42 cm^{-1} and 1078.55 cm^{-1} for TTM_2, and 1032.17 cm^{-1} and 1077.99 cm^{-1} for TTM_3.

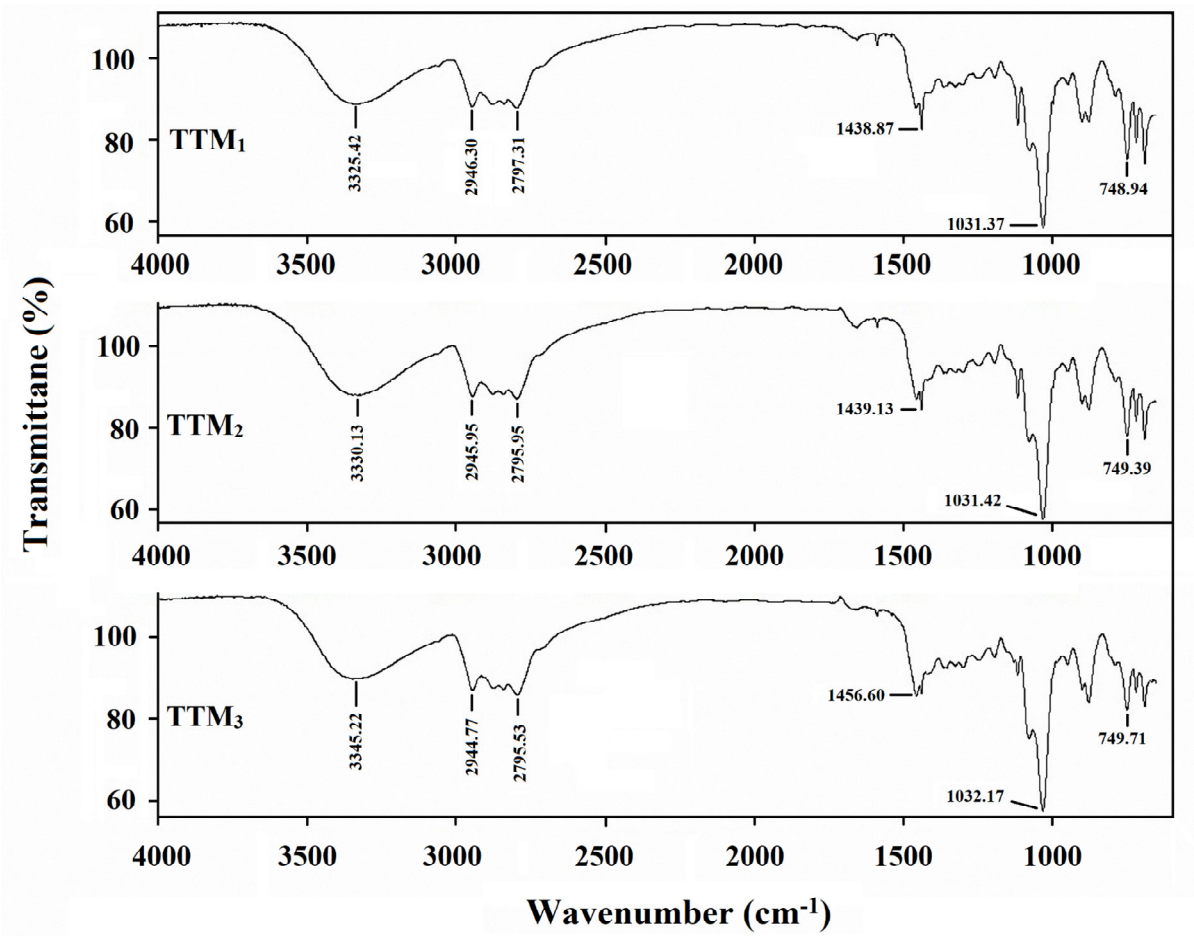

Fig. 1. FT-IR spectra for TTMs studied in this research work.

Thermal Stability Results

Fig. 2 displays the TGA curves of TTMs as well as their individual compounds. Generally, the T_{dcp} of HBAs is higher than that of HBDs.[66] As seen from Fig. 2, MTPPB had a higher T_{dcp} than MDEA and it is obvious that there was only one decomposition step in TGA curves of pure components (MTPPB and MDEA), while two decomposition steps occurred in TGA curves for all TTMs; then, there are two onset temperatures (T_{onset}). As is clear in Fig. 2, the first T_{onset} in TGA curves was almost the same, about 473 K, indicating the T_{dcp} of MDEA. At the first decomposition step, TTM_1 has a lower weight loss compared to TTM_2 and TTM_3. By continuing the heating at a constant rate, the second decomposition step can be observed. The TTM_3 exhibited the lowest

second T_{onset} in the TGA curve. The second step is pertinent to the T_{dcp} of MTPPB because the HBA is more stable than HBD and decomposes later.

Several researchers have used the T_{dcp} at 10% weight loss ($T_{10\%}$) as an accurate method to analyze the stability of materials.[67-69] Because of two degradation steps, T_{dcp} at 90% weight loss ($T_{90\%}$) is also reported for better comparison. All TTMs had a $T_{10\%}$ value of about 433 K. The values of $T_{90\%}$ for TTM_1, TTM_2, TTM_3 were 677 K, 663.24 K, and 625.03 K, respectively. Therefore, it can be interpreted that increasing the MDEA concentration in mixtures decreased their thermal stability.

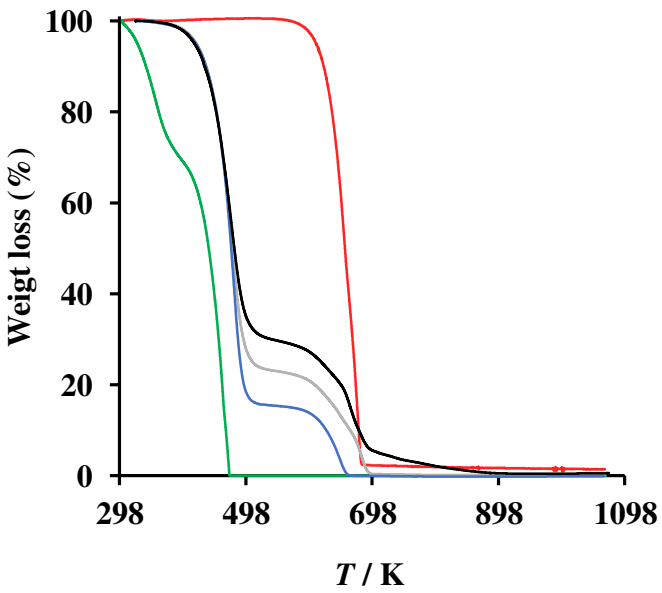

Fig. 2. Dynamic TGA curves for single components and TTMs. Lines represent: (—) MDEA, (—) MTPPB, (—) TTM_1, (—) TTM_2, (—) TTM_3.

Viscosity Results

The experimental viscosity data of MDEA and TTMs are summarized in Table S5, and shown in Fig. S4. From the data in Table S5 and Fig. S4, it is evident that the viscosity of MDEA is lower than that of TTMSs. Table S5 also presents a comparison between the viscosity of MDEA in this research work and the literature.[70-72] The low average absolute deviation (*%AAD*) value of 0.1429 indicates the consistency between experimental viscosity and literature data.[73,74]

According to ANOVA results presented in Table S6, both temperature and HBA mass fraction had a great effect on the viscosity, however, the effect of temperature was more significant than that of HBA mass fraction. Fig. 3 manifests three-dimensional (3-D) surface plots for viscosity was created based on the transformed quadratic model (see Table S6) As shown in Fig. 3, the viscosity data decreased upon decreasing the HBA concentration at any constant temperature. Indeed, a larger quantity of HBD in the mixture resulted in increased OH stretching bonds; then the hydrogen bonding interactions became weaker. As a result, the viscosity of TTMs decreased. A similar result was observed in the previous work.[46] Typically, as the temperature increased up to 323.15 K, the viscosity of TTMs decreased dramatically at any constant HBA mass fraction, further raising temperature did not have much effect on the viscosity. [46]

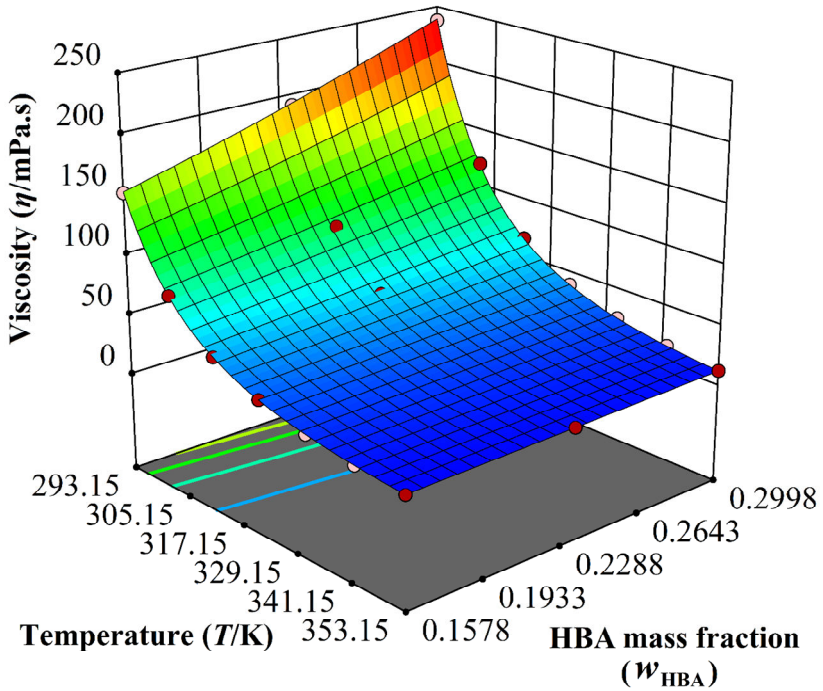

Fig. 3. 3-D plot of viscosity data against temperature and HBA mass fraction.

The following empirical equation was used to correlate experimental η data:[27,46,75]

$$\ln(\frac{\eta}{\rho M_{\mathrm{TTM}}}) = A_0 + \frac{A_1}{T} + \frac{A_2}{T^2} + \ldots \frac{A_n}{T^n} = \sum_{\mathrm{i}=0}^{\mathrm{n}} \frac{A_i}{T^i} \qquad (1)$$

where T and ρ stand for temperature and density of TTM (available in previous work[28]), respectively; A_{i} is the fitting parameter; M_{TTM} is molecular weight of TTM in g.mol^{-1}.

In addition to the above equation, several equations such as Arrhenius, Vogel-Fulcher-Tammann (VTF), Andrade, Waterton, Seddon and Yaws were used to correlate the experimental viscosity with temperature, as mentioned in the Supporting Information. A Levenberg-Marquardt method based on the nonlinear least-squares algorithm was used to derive the fitting parameters of equations together with root mean square error (*RMSE*) and coefficient determination (R^2) values, as presented in Table S7. The solid lines in Fig. S4 represent the calculated viscosity data via Eq. (1). As seen in Fig. S4 and Table S7, Eq. (1) suitably correlated the experimental viscosity data indicating high accuracy of this equation.

The experimental η data were used to estimate the energy barrier (E, J.mol^{-1}) of TTMs. If the E data is higher, the ions hardly move past each other, which can be inherently associated with the interactions occurring in the fluid.[76,77] This is an indication of a highly viscous fluid. Eq. (2) was used for calculation of E:[46]

$$E = R \times \frac{\partial(\ln[\eta\,(T)])}{\partial(1/T)} = R \times (A_1 + \frac{2A_2}{T}) \qquad (2)$$

where E is the energy barrier of TTM in J.mol^{-1}; η is the viscosity of solvents in mPa.s; T and R are temperature in K and the gas constant in J.mol^{-1}. K^{-1}, respectively; A_1 and A_2 are fitting parameters, as presented in Table S7. The calculated E data obtained from fitting parameters are set out in Table 2. As Table 2 shows, the E values decreased moderately with an increase in temperature. Moreover, it is observed that TTM_1 had a higher activation energy than the other studied TTMs indicating higher viscosity of this solvent.

By applying Eyring's absolute rate theory, the viscosity of a liquid is expressed via:[78-80]

$$\eta = \frac{h.N_A}{V}\exp\left(\frac{\Delta G^*}{RT}\right) \quad (3)$$

where V is molar volume of TTMs (and available in previous work[28]); h and N_A stand for Planck's constant and Avogadro's number, respectively; R and T are the universal gas constant and temperature, respectively; and ΔG^* is the molar Gibbs free energy of activation which was determined from Eq. (4):

$$\Delta G^* = \Delta H^* - T.\Delta S^* \quad (4)$$

Combining Eq. (4) with Eq. (3), the viscosity of liquid estimated as:

$$R.\ln(\frac{\eta.V}{h.N_A}) = \frac{\Delta H^*}{T} - \Delta S^* \quad (5)$$

In Eqs. (4) and (5) ΔS^* and ΔH^* are the entropy and enthalpy of viscous flow, respectively. Depending on liquids, there is a linear relationship between R.ln ($\eta.V/h.N_A$) and $1/T$; then, ΔH^* is obtained from the slope and ΔS^* from the intercept. Here, however, there was a curvature by plotting R.ln($\eta.V/h.N_A$) vs. $1/T$, as displayed in Fig. S5. These results show that ΔH^* is not independent of temperature for DESs. Therefore, the following polynomial fitting equation was used to determine thermodynamic properties:

$$R.\ln(\frac{\eta.V}{h.N_A}) = \beta_1 + \frac{\beta_2}{T} + \frac{\beta_3}{T^2} = \sum_{i=1}^{3}\frac{\beta_i}{T^{i-1}} \quad (6)$$

where β_1, β_2, and β_3 are adjustment coefficients.

The ΔH^* and ΔS^* values were obtained by the following equations:

$$\Delta H^* = \beta_2 + \frac{2\beta_3}{T} \quad (7)$$

$$\Delta S^* = -\beta_1 + \frac{\beta_3}{T^2} \quad (8)$$

The ΔH^*, ΔS^* and ΔG^* values are presented in Table 2. It can be seen from the data in Table 2 that TTM_1 has higher ΔH^*, ΔS^*, and ΔG^* values than the other TTMs. It is evident that with an increase in the temperature and molar ratio of TTMs, these properties experienced an decreased trend in the value. The highest values of these activation parameters were observed at 293.15 K in the case of TTM_1 while their lowest values occurred at 353.15 K for TTM_3.

A positive (+) ΔS^* change means an increase in disorder. The positive values of ΔH^* and ΔS^* are in good agreement with those of DESs in the previous work.[46] From Table 2, it can be found that the magnitude of ΔH^* is higher than $T.\Delta S^*$ values. This indicates that the energetic contribution, corresponding to ΔH^*, is more significant than the entropic contribution terms to ΔG^* values.[81] Therefore, for these investigated systems in this study, it seems that the interactional factor is predominant over the structural one.

Table 2 . Energy Barrier (E /J.mol^{-1}), Enthalpy of Viscous Flow (ΔH^* /J.mol^{-1}), Entropy of Viscous Flow (ΔS^*/J.mol^{-1}.K^{-1}) and Molar Gibbs Free Energy (G^* / J mol^{-1}) for TTMs in this Research Work

T (K)	E (J.mol^{-1})			ΔH^* (J.mol^{-1})			ΔS^* (J.mol^{-1}.K^{-1})			G^* (J mol^{-1})		
	TTM_1	TTM_2	TTM_3	TTM_1	TTM_2	TTM_3	TTM_1	TTM_2	TTM_3	TTM_1	TTM_2	TTM_3
293.15	51355.4	49164.8	47135.5	51369.03	49168.08	47104.69	81.477	76.106	71.269	27484.1	26857.7	26212.1
303.15	47856.4	45955.9	44199.8	47869.48	45958.84	44170.02	69.736	65.339	61.423	26729.1	26151.4	25549.5
313.15	44581.0	42951.9	41451.6	44593.43	42954.56	41422.77	59.102	55.587	52.506	26085.7	25547.5	24980.6
323.15	41508.2	40133.9	38873.4	41520.14	40136.23	38845.55	49.439	46.726	44.403	25543.8	25036.7	24496.7
333.15	38620.0	37485.0	36450.1	38631.34	37487.08	36423.06	40.634	38.651	37.019	25094.1	24610.4	24090.1
343.15	35900.0	34990.5	34168.0	35910.92	34992.34	34141.75	32.587	31.272	30.271	24728.6	24261.3	23754.2
353.15	33334.2	32637.3	32015.1	33344.56	32638.88	31989.64	25.214	24.511	24.088	24440.1	23982.9	23482.8

Surface Tension Results

Table S8 presents the surface tension (γ) data of MDEA and TTMs and Fig. S6 depicts these data as a function of temperature. From the data in Table S8 and Fig. S6, TTMs had a lower surface tension value than MDEA. Table S8 also compares the γ of MDEA in this research work and the literature. The low *%AAD* value of 0.2303 indicating a well agreement between experimental γ and literature data.

The experimental γ values were correlated using Eq. (9):

$$\ln\left(\frac{\gamma}{\rho \times M_{\mathrm{TTM}}}\right) = A_0 + \frac{A_1}{T} + \frac{A_2}{T^2} + \ldots \frac{A_n}{T^n} = \sum_{\mathrm{i}=0}^{\mathrm{n}} \frac{A_i}{T^i} \qquad (9)$$

where ρ and M_{TTM} represent the density and molecular weight of TTM, respectively; T is the temperature in K, and A_{i} is the fitting parameter. The solid lines in Fig. S6 are the calculated surface tension data using Eq. (9). Table S9 lists the fitting parameters, *RMSE* and R^2. From the correlation results shown in Table S9 and Fig. S7, it is clear that Eq. (9) can correlate the experimental γ data satisfactorily and suitably with R^2 of more than 0.99.

The main factors which have a great effect on γ data are temperature and hydrogen bonding between HBA and HBD. Hydrogen bonds provide higher γ to a liquid. Table S10 presents the ANOVA results for surface tension response. According to the ANOVA results, although both temperature and HBA mass fraction were highly significant with a p-value of less than 0.0001, temperature had a higher effect on the surface tension of TTMs. The effect of temperature and HBD mass fraction on the surface tension is illustrated in Fig. 4. It is obvious from Fig. 4 that as the temperature increased the γ values decreased linearly due to the disruption of hydrogen bonds in the liquids. There was a decreasing trend in the surface tension data as the HBA mass fraction (the ATPPB concentration) decreased in the mixture. As mentioned earlier, the hydrogen bonding between HBA and HBD was more strong in the case of TTM_1, therefore, it is expected to have a

higher surface tension in comparison to TTM_2, and TTM_3 over the temperature range. These results are in good agreement with previous results reported for DESs.[46]

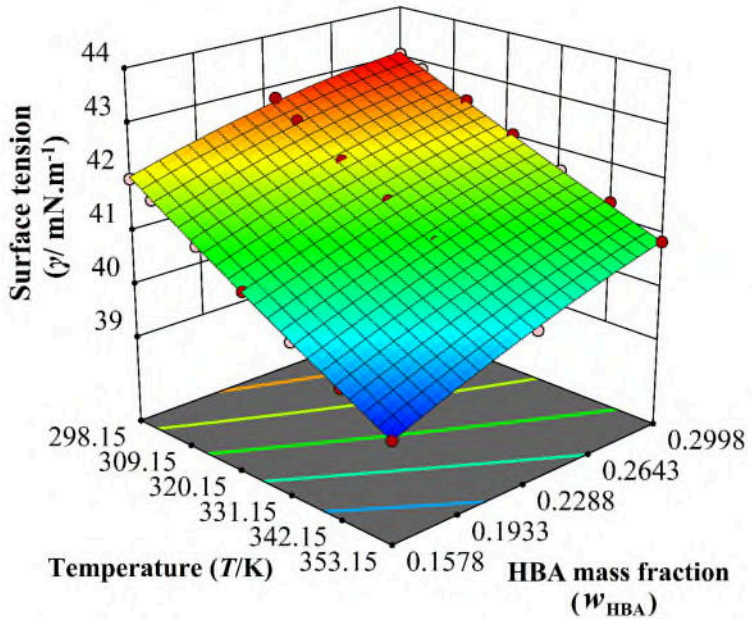

Fig. 4. 3-D plot of surface tension data against temperature and HBA mass fraction.

In order to understand the interactions between different components, the derived surface thermodynamic properties including surface entropy (S^{γ}) and internal surface energy (U^{γ}) are important.[46] Then, Gibbs-Helmholtz expressions were applied to obtain the surface thermodynamic properties:[46]

$$S^{\gamma} = -\left(\frac{\partial \gamma}{\partial T}\right)_P \qquad (10)$$

$$U^{\gamma} = \gamma - S^{\gamma} = \gamma - T \times \left(\frac{\partial \gamma}{\partial T}\right)_P \qquad (11)$$

where S^{γ} and U^{γ} represent the surface entropy and internal surface energy, respectively; P and T are pressure and temperature, respectively. In order to evaluate the S^{γ} and U^{γ}, the experimental γ values

were linearly fitted with respect to T. As presented in Table 3, the S^{γ} values of all TTMs are very close to each other and remarkably low, particularly when these values are compared with traditional molecules (i.e. alcohols and water),[82] as well as some DESs.[46] There are increasing trends on the S^{γ} values with increasing molar ratio of TTMs. Similar results were reported in the case of DESs.[46]

It is evident from Table 4 that with an increase in the temperature and molar ratio (or moles of HBD), the U^{γ} values of the TTMs decreased; hence, TTM_1 had higher U^{γ} values than TTM_2 and TTM_3 over the entire temperature range studied here.

Table 3 . The Derived Surface Entropy (S^{γ}/mJ.m^{-2}.K^{-1}) of TTMs Using Eq. (10) along with *RMSE* and R^2 Values

Solvent	S^{γ} (mJ.m^{-2} .K^{-1})	*RMSE*	R^2
TTM_1	0.03975	0.0225	0.9994
TTM_2	0.04841	0.0267	0.9994
TTM_3	0.05096	0.0262	0.9995

Table 4 . The Derived Internal Surface Energy (U^{γ}/ mJ.m^{-2}) of TTMs Using Eq. (11) at Several Temperatures

T (K)	TTM_1	TTM_2	TTM_3
293.15	31.21	28.37	26.80
303.15	30.82	27.82	26.29
313.15	30.03	26.84	25.24
323.15	29.22	25.89	24.24
333.15	28.40	24.93	23.17
343.15	27.67	23.97	22.22
353.15	26.83	23.01	21.19

3.1 Estimated critical temperatures

Since many corresponding state correlations include the critical temperatures (T_c), calculation of this thermo-physical property is highly important. Several approaches have been reported for prediction of the T_c in the literature, namely the Valderrama, Robles, Eötvos and Guggenheim relations.[83-87] A result reported by Freire *et al.* showed that using Robles and Valderrama relations are unreliable for estimating the T_c of some imidazolium-based ILs.[83] Therefore, in this research work, Eötvos and Guggenheim relations were applied to estimate the T_c of TTMs, as given below:[46]

Eötvos equation:

$$\gamma \times (V)^{2/3} = K(T_c - T) \quad (12)$$

Guggenheim equation:

$$\gamma = \gamma_0 \left(1 - \frac{T}{T_c}\right)^{11/9} \quad (13)$$

where V is the molar volume of TTMs in g.cm^{-3} which is determined from $V=M_{TTM}/\rho$ (M_{TT} and ρ are the molecular weight and density of TTM, respectively); γ_0 and T_c are an empirical parameter characteristic of the TTMs and the critical temperature, respectively. Since 11/9 is close to 1, Eq. (13) is simplified to $\gamma = \gamma_0 - \gamma_0 T/T_c$. Therefore, by raising the temperature, the γ data will decrease and go linearly to zero at a critical point.[88] Finding the γ and ρ data at the same experimental conditions in the literature is the main limitation of using Eötvos equation. Table 5 lists the calculated T_c values of TTMs by the Eötvos and Guggenheim equations. The T_c of MDEA is 667.5 K and is lower than all the TTMs. Therefore, as MDEA concentration increases in the mixture, T_c values of liquids decreases towards T_c of MDEA, as presented in Table 5. TTM_1 had a higher T_c value than TTM_2 and TTM_3 due to the strongest hydrogen bonds in TTM_1.

As seen from Table 5, there is a difference between predicted T_c of TTMs using the Eötvos and Guggenheim empirical equations. Therefore, it is important to understand the reliability and accuracy of these equations and to investigate which calculated T_c is reliable. To do so, the modified Rackett equation was employed as given below:[46]

$$\ln\rho = \ln a - [\ln b.(1 - T/T_C)^n] \quad (14)$$

where ρ is the density of TTMs in g.cm^{-1}; T_c is critical temperature in K; a, b, and n represent regression coefficients. Table S11 lists all coefficients along with R^2 and *RMSE*. According to the data in Table S11, although there is good agreement between calculated and experimental density data using calculated T_c by both Eötvos and Guggenheim equations, using Guggenheim equation for calculating T_c of TTMs is slightly more accurate than Eötvos equation. The same results were achieved for DESs.[46]

Table 5 . Estimated Critical Temperatures (T_c / K) Using Equations of Eötvos and Guggenheim along with *RMSE* and R^2 Values

	Eötvos equation, Eq. (12)			Guggenheim equation Eq. (13)		
Solvent	T_c (K)	R^2	*RMSE*	T_c (K)	R^2	*RMSE*
TTM_1	2317	0.9977	0.604	1616	0.9994	0.0093
TTM_2	1735	0.9987	0.607	1372	0.9995	0.0105
TTM_6	1603	0.9988	0.612	1299	0.9995	0.0105

CO_2 Solubility in TTMs

Table 6 provides the data on CO_2 solubility in solvents at 303.15 K and pressure up to 1.35 MPa are presented in. As can be seen from Table 6, by increasing the pressure, the CO_2 solubility in TTMs increased, as is typically expected for gas solubility in liquids. The most striking result to emerge from the data in Table 6 is that there was no direct relationship between molar ratio and CO_2 solubility and no increase in CO_2 solubility was detected for solvent with molar ratio 1:16. According to Table 6, the CO_2 solubility in TTMs followed this order: TTM_2>TTM_1>TTM_3.

Indeed, by increasing the amount of MDEA in mixtures, the CO_2 solubility increased in TTM_2 and then decreased in TTM_3. Therefore, TTM_2 exhibited a higher CO_2 absorption compared with TTM_1 and TTM_3.

A number of studies have examined the effect of increasing quantity of amines as HBDs in mixtures on CO_2 solubility. Ali *et al.* stated that increased MEA moles in MTPPB-MEA mixture decreased the CO_2 solubility in this DES.[89] However, other researchers have reported different stories. Adeyemi *et al.* measured the CO_2 solubility in a mixture of choline chloride-MDEA (ChCl-MDEA) in different molar ratios of 1:6, 1:8 and 1:10 at 313.15 K.[90] Their results showed that by increasing the quantity of MDEA in the mixture, CO_2 absorption increased. They did not investigate the CO_2 solubility in higher molar ratios of ChCl-MDEA mixture (for example 1:16). A similar result was reported by Sarmad *et al.* who measured CO_2 solubility in tetrapropylammonium chloride-ethanolamine in molar ratios of 1:4 and 1:7 HBA/HBD and tetrabutylammonium bromide-ethanolamine with two molar ratios of 1:6 and 1:7 HBA/HBD.[91] The CO_2 uptake in several DESs was reported by Shukla *et al.* who used monoethanolammonium chloride, 1-methylimidazolium chloride and tetra-n-butylammonium bromide as HBAs and ethylenediamine (EDA) and 3-amino-1-propanol (AP) as HBDs with molar ratios of 1:1, 1:2, 1:3, and 1:4 HBA to HBD.[92] Their results revealed that CO_2 uptake was improved by increasing the molar ratio of HBA/HBD from 1:1 to 1:4. They also did not report the CO_2 uptake at higher molar ratios of DESs.

On the other hand, the same mixtures of MEACl-EDA with the same molar ratios of 1:1, 1:2, 1:3, and 1:4 HBA to HBD were prepared by Trivedi *et al.* for CO_2 capture. [93] After 3 hours, MEACl-EDA 1:3 ratio exhibited the highest CO_2 uptake (mole CO_2/mole solvent) at 303.15 K compared with other DESs. Unlike the result obtained by Shukla *et al.*,[92] they pointed out that there is no direct relationship between CO_2 solubility and molar ratio and an increase in EDA concentration in the mixture (4-mole) had a negative effect on the CO_2 uptake so that it decreased slightly. Therefore,

in light of the above-mentioned findings, it can be inferred that there is no direct relationship between increasing the fraction of amine as HBD in the mixture and increasing CO_2 solubility.

It is elucidated from Table 6 that the CO_2 loading capacity (a_{CO_2}) of TTM increased with an increase in MDEA concentration up to 10:1 mole ratio, and further increase in MDEA concentration suppressed the a_{CO_2} of TTM. Like MDEA, these solvents had an equilibrium loading capacity approaching 1 mole CO_2 per mole TTM at higher pressure. This indicates that the nature of HBD plays an important role in the CO_2 solubility process because MDEA has a high CO_2 loading capacity.

Table 6 . The CO_2 Solubility Results at 303.15 in this Research Work

Solvent	P^E (MPa)	x_{CO_2}	a_{CO_2}
TTM_1			
	0.660	0.4090	0.6919
	0.826	0.4333	0.7646
	1.009	0.4525	0.8266
	1.351	0.5052	1.0211
TTM_2			
	0.597	0.3934	0.6484
	0.797	0.4284	0.7494
	0.896	0.4525	0.8264
	1.230	0.5131	1.0539
TTM_3			
	0.615	0.3816	0.6172
	0.816	0.4234	0.7343
	0.982	0.4396	0.7845
	1.243	0.4821	0.9311

A comparison between CO_2 solubility in ILs and DESs and that in TTM_2 is shown in Fig. 5. To do so, CO_2 solubility data were collected in trihexyltetradecylphosphoniump [THTDP]-based IL with anion of bis(trifluoromethyl)sulfonylimide ($[NTf_2]^-$) and several imidazolium-based ILs containing cations such as 1-ethyl-3 methylimidazolium ($[C_2mim]^+$), 1-(2-hydroxyethyl)-3-methylimidazolium ($[C_6mim]^+$) and 1-octyl-3-methylimidazolium ($[C_8mim]^+$) and different anions,

for instance, $[NTf_2]^-$, hexafluorophosphate ($[PF_6]^-$), trifluoromethanesulfonate ($[OTf]^-$), tetrafluoroborate ($[BF_4]^-$), ethylsulfate ($[EtSO_4]^-$), and bis(trifluoromethyl)sulfonylimide ($[NTf_2]^-$) as well as two types of phosphonium-based DESs comprising HBA of allyltriphenylphosphonium bromid (ATPPB) different HBDs of TEG and DEG. [50,94-99] As can be seen from Fig. 5, the solvent studied in this research work, TTM_2, exhibited higher CO_2 solubility in comparison to ILs and DESs. So far, in the literature, solvents amongst DESs and TTMs with better CO_2 absorption performance than solvents studied here cannot be found.

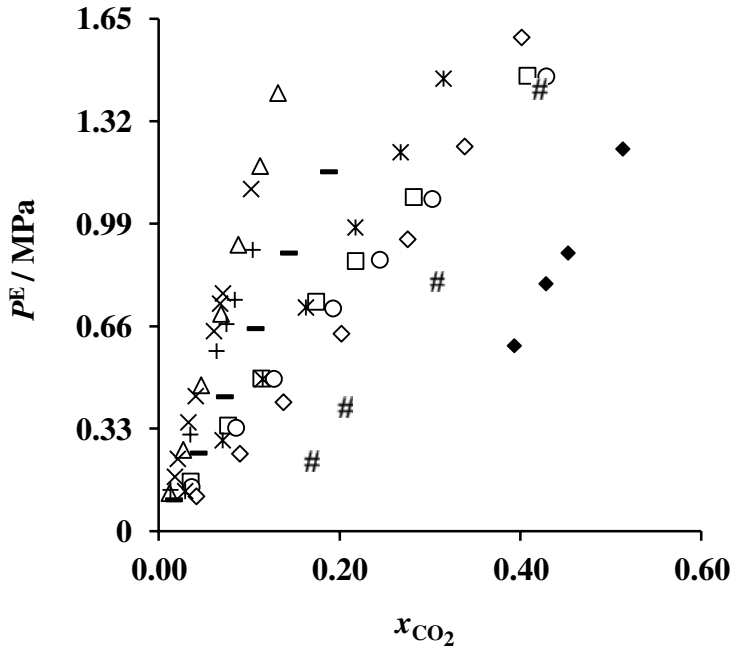

Fig. 5. A comparison of CO_2 solubility in TTM_2 in this research work with that in ILs and DESs at 303.15 K. Symbols are: (♦) TTM_2; (□) ATPPB-TEG 1:4;[50] (○) ATPPB-DEG 1:4;[50] (#) [THTDP][NTf_2];[94] (×) [C_6mim][BF_4];[95] (–) [C_6mim][OTf];[96] (+) [C_6mim][PF_6];[96] (*) [C_8mim][PF_6];[97] (Δ) [C_2mim][$EtSO_4$];[98] and (◊) [C_8mim][NTf_2].[99]

▪ CONCLUSIONS

In this research work, new transition-temperature mixtures were synthesized for CO_2 capture by mixing MTPPB as a HBA and MDEA as a HBD in three molar ratios of 1:7, 1:10, and 1:16 HBA to HBD. Since these solvents are new, collecting the fundamental thermo-physical data is

necessary. The FT-IR analysis showed that TTMs had similar spectra and chemical compositions with different levels of transmittance. Moreover, it was found that solvent containing lower MDEA concentration had a lower wavenumber of OH stretching vibration. Thermal stability results disclosed that as the MDEA concentration in the mixture increased the thermal stability of TTMs decreased towards the lower thermal stability of MDEA. The viscosity and surface tension of solvents and MDEA were measured at atmospheric pressure and temperature up to 343.15 K. It was observed that, with an increase of temperature and addition of MDEA in mixtures, both viscosity and surface tension of TTMs decreased. Experimental viscosity values were used to calculate activation parameters of TTMs based on Eyring's absolute rate theory such as molar Gibbs free energy of activation, the enthalpy, and entropy of viscous flow. The experimental surface tension data were used to calculate the critical temperatures of TTMs and their surface thermodynamic properties such as surface entropy and internal surface energy. The result indicated that TTM_1 had higher critical temperatures because of strong hydrogen bonding. In order to study the effect of temperature (T/K) and HBA mass fraction (w_{HBA}) on the viscosity and surface tension of TTMs, a response surface methodology (RSM) was applied and the results revealed that both factors had a significant effect on the studied properties. Finally, CO_2 solubility data showed that TTM_2 exhibited the highest CO_2 absorption amongst all TTMs studied here at 303.15 K and had an equilibrium loading capacity of 1 mole CO_2/mole TTM at a pressure of 1 MPa. The present research work demonstrates that these studied solvents possess a greater affinity for CO_2 and higher CO_2 absorption performance compared with other TTMs and DESs reported in the literature up to now and they can be regarded as solvents with high potential for CO_2 capture.

Notes

The authors declare no competing financial interest

▪ ACKNOWLEDGMENTS

Ghaedi H. and Zhao M. are grateful for the support of National Natural Science Foundation of China (grant number: 51506112) and Tsinghua University Initiative Scientific Research Program (grant number: 20161080094). The authors would like to thank the team of the Solvent Development Lab of Research Centre for CO_2 Capture ($RCCO_2C$) at the Universiti Teknologi Petronas of Malaysia for their support.

▪ REFERENCES

(1) Oceanography, S. I. o.; Mauna Loa Oservatory 2018.
(2) Pachauri, R. K.; Reisinger, A., Climate Change 2007: Synthesis Report. [Online]. Geneva, Switzerland, 2007.
(3) Sneddon, G.; McGlynn, J. C.; Neumann, M. S.; Aydin, H. M.; Yiu, H. H. P.; Ganin, A. Y. *Journal of Materials Chemistry A* **2017**, *5*, 11864-11872.
(4) Nawar, A.; Ghaedi, H.; Ali, M.; Zhao, M.; Iqbal, N.; Khan, R. *Process Safety and Environmental Protection* **2019**.
(5) Luis, P. *Desalination* **2016**, *380*, 93-99.
(6) Mandal, B. P.; Bandyopadhyay, S. S. *Chemical Engineering Science* **2006**, *61*, 5440-5447.
(7) Derks, P.; Dijkstra, H.; Hogendoorn, J.; Versteeg, G. *AIChE journal* **2005**, *51*, 2311-2327.
(8) Idem, R.; Wilson, M.; Tontiwachwuthikul, P.; Chakma, A.; Veawab, A.; Aroonwilas, A.; Gelowitz, D. *Industrial & Engineering Chemistry Research* **2005**, *45*, 2414-2420.
(9) Mandal, B. P.; Guha, M.; Biswas, A. K.; Bandyopadhyay, S. S. *Chemical Engineering Science* **2001**, *56*, 6217-6224.
(10) Bara, J. E. *Greenhouse Gases: Science and Technology* **2012**, *2*, 162-171.
(11) Rao, A. B.; Rubin, E. S. *Environmental Science & Technology* **2002**, *36*, 4467-4475.
(12) Thitakamol, B.; Veawab, A.; Aroonwilas, A. *International Journal of Greenhouse Gas Control* **2007**, *1*, 318-342.
(13) Yu, C.-H.; Huang, C.-H.; Tan, C.-S. *Aerosol and Air Quality Research* **2012**, *12*, 745-769.
(14) Mondal, M. K.; Balsora, H. K.; Varshney, P. *Energy* **2012**, *46*, 431-441.
(15) Murshid, G.; Ghaedi, H.; Ayoub, M.; Garg, S.; Ahmad, W. *J. Mol. Liq.* **2018**, *250*, 162–170.
(16) Murshid, G.; Ghaedi, H.; Ayoub, M.; Mjalli, F. S.; Garg, S. *J. Env. Chem. Eng.* **2018**, *6*, 6390-6398.
(17) Nikolaeva, D.; Azcune, I.; Sheridan, E.; Sandru, M.; Genua, A.; Tanczyk, M.; Jaschik, M.; Warmuzinski, K.; Jansen, J. C.; Vankelecom, I. F. J. *Journal of Materials Chemistry A* **2017**, *5*, 19808-19818.
(18) Xu, X.; Heath, C.; Pejcic, B.; Wood, C. D. *Journal of Materials Chemistry A* **2018**, *6*, 4829-4838.
(19) Yang, J.; Tan, H. Y.; Low, Q. X.; Binks, B. P.; Chin, J. M. *Journal of Materials Chemistry A* **2015**, *3*, 6440-6446.
(20) Gardas, R. L.; Coutinho, J. A. P. *Fluid Phase Equilibria* **2008**, *266*, 195-201.
(21) Bara, J. E.; Carlisle, T. K.; Gabriel, C. J.; Camper, D.; Finotello, A.; Gin, D. L.; Noble, R. D. *Industrial & Engineering Chemistry Research* **2009**, *48*, 2739-2751.
(22) Zubeir, L. F.; Lacroix, M. H. M.; Kroon, M. C. *The Journal of Physical Chemistry B* **2014**, *118*, 14429-14441.
(23) Zakrzewska, M. E.; Bogel-Łukasik, E.; Bogel-Łukasik, R. *Energy & Fuels* **2010**, *24*, 737-745.
(24) Abbott, A. P.; Capper, G.; Davies, D. L.; Rasheed, R. K.; Tambyrajah, V. *Chemical Communications* **2003**, 70-71.
(25) Francisco, M.; van den Bruinhorst, A.; Kroon, M. C. *Green Chemistry* **2012**, *14*, 2153-2157.
(26) Aissaoui, T.; AlNashef Inas, M.; Qureshi Umair, A.; Benguerba, Y. In *Rev. Chem. Eng.*, 2017, p 523.
(27) Ghaedi, H.; Ayoub, M.; Sufian, S.; Shariff, A. M.; Lal, B.; Wilfred, C. D. *The Journal of Chemical Thermodynamics* **2018**, *118*, 147–158.
(28) Ghaedi, H.; Zhao, M.; Ayoub, M.; Zahraa, D.; Mohd Shariff, A.; Inayat, A. *The Journal of Chemical Thermodynamics* **2019**, *137*, 108-118.
(29) Francisco, M.; van den Bruinhorst, A.; Kroon, M. C. *Angew. Chem. Int. Ed.* **2013**, *52*, 3074-3085.
(30) Rodríguez, N. R.; González, A. S. B.; Tijssen, P. M. A.; Kroon, M. C. *Fluid Phase Equilib.* **2015**, *385*, 72-78.
(31) Ma, S.; Hou, Y.; Sun, Y.; Li, J.; Li, Y.; Sun, L. *Chemical Engineering and Processing: Process Intensification* **2017**, *121*, 71-80.
(32) Kottaras, P.; Koulianos, M.; Makris, D. P. *Recycling* **2017**, *2*, 3.
(33) Tereshatov, E. E.; Boltoeva, M. Y.; Folden, C. M. *Green Chemistry* **2016**, *18*, 4616-4622.
(34) Karageorgou, I.; Grigorakis, S.; Lalas, S.; Makris, D. P. *Eur. Food Res. Technol.* **2017**, *243*, 1839-1848.
(35) Dedousi, M.; Mamoudaki, V.; Grigorakis, S.; Makris, D. P. *Environments* **2017**, *4*, 31.

(36) Yiin, C. L.; Quitain, A. T.; Yusup, S.; Sasaki, M.; Uemura, Y.; Kida, T. *Bioresour. Technol.* **2016**, *199*, 258-264.
(37) Yiin, C. L.; Quitain, A. T.; Yusup, S.; Uemura, Y.; Sasaki, M.; Kida, T. *Bioresour. Technol.* **2017**, *244*, 941-948.
(38) Liu, J.; Wang, J.; Fu, Y.; Chang, J. *RSC Adv.* **2016**, *6*, 94588-94594.
(39) Bao, Q.; Zhao, L.; Jing, H.; Mao, A. *Materials Today Communications* **2018**, *14*, 249-253.
(40) Francisco, M.; van den Bruinhorst, A.; Zubeir, L. F.; Peters, C. J.; Kroon, M. C. *Fluid Phase Equilib.* **2013**, *340*, 77-84.
(41) Bougie, F.; Iliuta, M. C. *Journal of Chemical & Engineering Data* **2012**, *57*, 635-669.
(42) Ma'mun, S.; Svendsen, H. F. *IOP Conference Series: Materials Science and Engineering* **2018**, *358*, 012011.
(43) Ghaedi, H.; Ayoub, M.; Sufian, S.; Lal, B.; Shariff, A. M. *The Journal of Chemical Thermodynamics* **2017**, *113*, 41-51.
(44) Paredes, X.; Fandiño, O.; Comuñas, M. J. P.; Pensado, A. S.; Fernández, J. *The Journal of Chemical Thermodynamics* **2009**, *41*, 1007-1015.
(45) Tariq, M.; Carvalho, P. J.; Coutinho, J. A. P.; Marrucho, I. M.; Lopes, J. N. C.; Rebelo, L. P. N. *Fluid Phase Equilib.* **2011**, *301*, 22-32.
(46) Ghaedi, H.; Ayoub, M.; Sufian, S.; Shariff, A. M.; Lal, B. *J. Mol. Liq.* **2017**, *241*, 500-510.
(47) Dawodu, O. F.; Meisen, A. *J. Chem. Eng. Data* **1994**, *39*, 548-552.
(48) Rho, S.-W.; Yoo, K.-P.; Lee, J. S.; Nam, S. C.; Son, J. E.; Min, B.-M. *Journal of Chemical & Engineering Data* **1997**, *42*, 1161-1164.
(49) Ghaedi, H.; Ayoub, M.; Sufian, S.; Murshid, G.; Farrukh, S.; Shariff, A. M. *International Journal of Greenhouse Gas Control* **2017**, *66*, 147-158.
(50) Ghaedi, H.; Ayoub, M.; Sufian, S.; Shariff, A. M.; Hailegiorgis, S. M.; Khan, S. N. *J. Mol. Liq.* **2017**, *243*, 564-571.
(51) Khan, S. N.; Hailegiorgis, S. M.; Man, Z.; Garg, S.; Shariff, A. M.; Farrukh, S.; Ayoub, M.; Ghaedi, H. *J. Mol. Liq.* **2018**, *249*, 1236-1244.
(52) Garg, S.; Shariff, A. M.; Shaikh, M. S.; Lal, B.; Aftab, A.; Faiqa, N. *Journal of Natural Gas Science and Engineering* **2016**, *34*, 864-872.
(53) Peng, D.-Y.; Robinson, D. B. *Industrial & Engineering Chemistry Fundamentals* **1976**, *15*, 59-64.
(54) Bogel-Łukasik, R.; Matkowska, D.; Bogel-Łukasik, E.; Hofman, T. *Fluid Phase Equilib.* **2010**, *293*, 168-174.
(55) Rangkooy, H. A.; Ghaedi, H.; Jahani, F. *J. Env. Chem. Eng.* **2019**, *7*, 103247.
(56) Abbas, Y.; Lu, W.; Wang, Q.; Dai, H.; Liu, Y.; Fu, X.; Pan, C.; Ghaedi, H.; Cheng, F.; Wang, H. *Environ. Pollut.* **2020**, 113944.
(57) Akbari, S.; Mahmood, M. S.; Ghaedi, H.; Al-Hajri, S. *Polymers* **2019**, *11*, 1-25.
(58) Akbari, S.; Mahmood, S. M.; Tan, I. M.; Hematpour, H. *Journal of Petroleum Exploration and Production Technology* **2018**, *8*, 887-900.
(59) Dastyar, W.; Zhao, M.; Yuan, W.; Li, H.; Ting, Z. J.; Ghaedi, H.; Yuan, H.; Li, X.; Wang, W. *ACS Sustainable Chemistry & Engineering* **2019**.
(60) Larkin, P. *Infrared and raman spectroscopy: principles and spectral interpretation*; Elsevier: Waltham, USA, 2011.
(61) Luo, J.; Conrad, O.; Vankelecom, I. F. J. *Journal of Materials Chemistry* **2012**, *22*, 20574-20579.
(62) AlOmar, M. K.; Hayyan, M.; Alsaadi, M. A.; Akib, S.; Hayyan, A.; Hashim, M. A. *Journal of Molecular Liquids* **2016**, *215*, 98-103.
(63) Hayyan, M.; Aissaoui, T.; Hashim, M. A.; AlSaadi, M. A.; Hayyan, A. *Journal of the Taiwan Institute of Chemical Engineers* **2015**, *50*, 24-30.
(64) Barceló, D. In *Comprehensive Analytical Chemistry*; Elsevier, 2001, pp 195-283.
(65) Song, W.; Zhao, Z.; Zheng, H.; Wang, G. *Water Science and Technology* **2013**, *68*, 1778.
(66) Abbas, Q.; Binder, L. *ECS Transactions* **2010**, *33*, 49-59.
(67) Wu, T.-Y.; Su, S.-G.; Gung, S.-T.; Lin, M.-W.; Lin, Y.-C.; Lai, C.-A.; Sun, I. W. *Electrochim. Acta* **2010**, *55*, 4475-4482.
(68) Shirota, H.; Mandai, T.; Fukazawa, H.; Kato, T. *Journal of Chemical & Engineering Data* **2011**, *56*, 2453-2459.
(69) Ghaedi, H.; Ayoub, M.; Sufian, S.; Lal, B.; Uemura, Y. *J. Mol. Liq.* **2017**, *242*, 395-403.
(70) Arachchige, U.; Aryal, N.; Eimer, D. A.; Melaaen, M. C. *Annual Transaction of the Nordic Rheology Society* **2013**, *21*, 299-306.
(71) DiGuilio, R. M.; Lee, R. J.; Schaeffer, S. T.; Brasher, L. L.; Teja, A. S. *Journal of Chemical & Engineering Data* **1992**, *37*, 239-242.
(72) Teng, T. T.; Maham, Y.; Hepler, L. G.; Mather, A. E. *Journal of Chemical & Engineering Data* **1994**, *39*, 290-293.
(73) Ghaedi, H.; Ayoub, M.; Sufian, S.; Hailegiorgis, S. M.; Murshid, G.; Farrukh, S.; Khan, S. N. *Thermochim. Acta* **2017**, *657*, 123-133.
(74) Ghaedi, H.; Ayoub, M.; Sufian, S.; Shariff, A. M.; Murshid, G.; Hailegiorgis, S. M.; Khan, S. N. *J. Mol. Liq.* **2017**, *248*, 378-390.
(75) Ghaedi, H.; Ayoub, M.; Sufian, S.; Hailegiorgis, S. M.; Murshid, G.; Khan, S. N. *The Journal of Chemical Thermodynamics* **2018**, *116*, 50-60.
(76) Okoturo, O. O.; VanderNoot, T. J. *J. Electroanal. Chem.* **2004**, *568*, 167-181.

(77) Martins, M. A. R.; Neves, C. M. S. S.; Kurnia, K. A.; Carvalho, P. J.; Rocha, M. A. A.; Santos, L. M. N. B. F.; Pinho, S. P.; Freire, M. G. *Fluid Phase Equilib.* **2016**, *407*, 188-196.
(78) Eyring, H. *The Journal of Chemical Physics* **1936**, *4*, 283-291.
(79) Kauzmann, W.; Eyring, H. *J. Am. Chem. Soc.* **1940**, *62*, 3113-3125.
(80) Vranes, M.; Dozic, S.; Djeric, V.; Gadzuric, S. *Journal of Chemical & Engineering Data* **2012**, *57*, 1072-1077.
(81) Ciocirlan, O.; Iulian, O.; Croitoru, O. *Rev Chim Bucharest* **2010**, *61*, 721-723.
(82) Gliński, J.; Chavepeyer, G.; Platten, J.-K.; Smet, P. *The Journal of Chemical Physics* **1998**, *109*, 5050-5053.
(83) Freire, M. G.; Carvalho, P. J.; Fernandes, A. M.; Marrucho, I. M.; Queimada, A. J.; Coutinho, J. A. P. *Journal of Colloid and Interface Science* **2007**, *314*, 621-630.
(84) Ali, K.; Shah, A.-u.-H. A.; Bilal, S.; Shah, A.-u.-H. A. *Colloids and Surfaces A: Physicochemical and Engineering Aspects* **2009**, *337*, 194-199.
(85) Shariati, A.; Ashrafmansouri, S.-S.; Osbuei, M. H.; Hooshdaran, B. *Korean Journal of Chemical Engineering* **2013**, *30*, 187-193.
(86) Valderrama, J. O.; Robles, P. A. *Industrial & Engineering Chemistry Research* **2007**, *46*, 1338-1344.
(87) Rebelo, L. P. N.; Canongia Lopes, J. N.; Esperança, J. M. S. S.; Filipe, E. *The Journal of Physical Chemistry B* **2005**, *109*, 6040-6043.
(88) Levine, I. N. *Physical Chemistry*, sixth ed.; McGraw-Hill: New York, 2009.
(89) Ali, E.; Hadj-Kali, M. K.; Mulyono, S.; Alnashef, I.; Fakeeha, A.; Mjalli, F.; Hayyan, A. *Chem. Eng. Res. Des.* **2014**, *92*, 1898-1906.
(90) Adeyemi, I.; Abu-Zahra, M. R. M.; Alnashef, I. *Energy Procedia* **2017**, *105*, 1394-1400.
(91) Sarmad, S.; Xie, Y.; Mikkola, J.-P.; Ji, X. *New J. Chem.* **2017**, *41*, 290-301.
(92) Shukla, S. K.; Mikkola, J.-P. *PCCP* **2018**, *20*, 24591-24601.
(93) Trivedi, T. J.; Lee, J. H.; Lee, H. J.; Jeong, Y. K.; Choi, J. W. *Green Chemistry* **2016**, *18*, 2834-2842.
(94) Carvalho, P. J.; Álvarez, V. H.; Marrucho, I. M.; Aznar, M.; Coutinho, J. A. P. *The Journal of Supercritical Fluids* **2010**, *52*, 258-265.
(95) Shokouhi, M.; Adibi, M.; Jalili, A. H.; Hosseini-Jenab, M.; Mehdizadeh, A. *Journal of Chemical & Engineering Data* **2010**, *55*, 1663-1668.
(96) Jalili, A. H.; Mehdizadeh, A.; Shokouhi, M.; Sakhaeinia, H.; Taghikhani, V. *The Journal of Chemical Thermodynamics* **2010**, *42*, 787-791.
(97) Safavi, M.; Ghotbi, C.; Taghikhani, V.; Jalili, A. H.; Mehdizadeh, A. *The Journal of Chemical Thermodynamics* **2013**, *65*, 220-232.
(98) Jalili, A. H.; Mehdizadeh, A.; Shokouhi, M.; Ahmadi, A. N.; Hosseini-Jenab, M.; Fateminassab, F. *The Journal of Chemical Thermodynamics* **2010**, *42*, 1298-1303.
(99) Jalili, A. H.; Safavi, M.; Ghotbi, C.; Mehdizadeh, A.; Hosseini-Jenab, M.; Taghikhani, V. *The Journal of Physical Chemistry B* **2012**, *116*, 2758-2774.

Cranfield University

CERES Research Repository **https://dspace.lib.cranfield.ac.uk/**

School of Water, Energy and Environment (SWEE) Staff publications (SWEE)

High CO2 absorption in new amine based-transition-temperature mixtures (deep eutectic analogues) and reporting thermal stability, viscosity and surface tension: Response surface methodology (RSM)

Ghaedi, Hosein

2020-07-23

Attribution-NonCommercial-NoDerivatives 4.0 International

Ghaedi H, Zhao M, Clough PT, et al., (2020) High CO2 absorption in new amine based-transition-temperature mixtures (deep eutectic analogues) and reporting thermal stability, viscosity and surface tension: Response surface methodology (RSM). Journal of Molecular Liquids, Volume 316, October 2020, Article number 113863

https://doi.org/10.1016/j.molliq.2020.113863

Downloaded from CERES Research Repository, Cranfield University